Roll-to-roll fabrication of three-dimensional self-folding microstructures

*Tongyao Wu, Ali Mehrnezhad, and Kidong Park**

Division of Electrical and Computer Engineering, Louisiana State University, Baton Rouge, LA 70803, USA

*E-mail: kidongp@lsu.edu

Keywords: self-folding, roll-to-roll, 3D microstructures, hollow microcarrier, cell culture

Abstract

Self-folding technology offers a promising alternative to conventional microfabrication techniques. It utilizes controlled and imbalanced stresses to transform specific patterns of flat materials into pre-determined three-dimensional (3D) structures for diverse applications. However, current production methods of self-folding structures are mostly limited to lab-scale production. In this study, a novel roll-to-roll (R2R) production setup is developed to address the limited scalability of self-folding technology. The R2R setup continuously stretches and bonds a pre-cured PDMS (polydimethylsiloxane) film to another PDMS film attached to a stiff PET (polyethylene terephthalate) carrier layer. This creates a bilayer PDMS film with imbalanced stress, causing it to self-fold into pre-determined 3D shapes upon patterning and releasing from the PET carrier layer. The R2R setup achieves a production rate of 96 cm^2/min, significantly surpassing our previous method based on spin-coating and baking. This demonstrates the potential of R2R technology for industrial-scale production of self-folding

microstructures.

Introduction

Self-folding technology[1-3] provides a novel alternative for fabricating complex three-dimensional (3D) microstructures, particularly those with hollow 3D geometries and thin walls. The term "self-folding" refers to a process in which specific patterns of thin flat film transform into pre-determined 3D structures by curving, rolling, or folding without external manipulation.[4] Microfabrication technology based on photolithography, deposition, and etching is widely used in fabricating micro/nano structures for integrated circuits, microelectromechanical systems, and microfluidic devices.[5] However, conventional microfabrication technology has a limited degree-of-freedom in thickness direction and is very challenging to fabricate 3D hollow structures. In contrast, the self-folding technique can easily generate fully 3D hollow structures, such as pyramids,[6] cubes,[6-9] spheres,[10] capsules,[11, 12] and tubes,[13-16] giving a new way to fabricate microstructures.

The fabrication of self-folding structures can be broadly categorized into two primary approaches.[17, 18] The first approach utilizes hinges that are locally deposited on patterned films. These hinges can shrink or expand to fold patterned films into 3D structures with sharp edges.[6-9] Alternatively, self-folding films,[3] or films with imbalanced residual stress can be used. Because the residual stress is spatially uniform in the films, the resulting self-folding structures often exhibit rounded shapes.[10-16, 19] Self-folding films are typically composed of a passive layer and an active layer. The passive layer provides structural rigidity for the entire structure, while the active layers bend the structure by either tensile or compressive stress.[20] The radius

of curvature (ROC) of the bending is determined by the residual stress within the films, as well as the thickness of each layer.[12]

The self-folding process can be triggered by external stimuli such as temperature,[21] solvent,[22] light,[23] electrical signal,[24] capillary forces,[25] and stress-release.[26] Smela and Jager et al. developed self-folding films made from a polymer layer and a gold layer that acted as electrically controllable hinges. With electrical stimulation, rigid plates with these hinges folded into or unfolded from cubes.[24, 27] Li et al. reported a dry-releasing approach using rapid thermal annealing to dehumidify a thin metal layer deposited on a pre-strained silicon monoxide and silicon dioxide bilayer film for the generation of surface tension and intrinsic strain, which rolled the film into nanotubes upon release.[26] Polymers are widely used to fabricate self-folding structures, as they have higher biocompatibility and response well to biochemical changes.[3, 28] For example, Ashkan et al. demonstrated hollow microcarriers (HMCs) fabricated with a self-folding bilayer PDMS (polydimethylsiloxane) film for adherent cell culture.[10] Zakharchenko et al. reported the fabrication of biodegradable tubes with polysuccinimide/polycaprolactone bilayers for tissue engineering scaffolds.[14] Other research explored self-folding films, showcasing their potential in various applications, such as drug encapsulation and delivery,[29] cell transportation and behavioral study of cells under confinement,[30] development of self-assembling microelectronic devices,[31] and scaffolds for tissue engineering.[32] Although the potential of self-folding technologies was clearly demonstrated in various applications, there have been very few studies on the large-scale production of the self-folding structures, which is essential in their commercialization.

The roll-to-roll (R2R) process shows great potential as a cost-effective and high-throughput fabrication process.[33-38] R2R technology encompasses a range of processes that utilize both additive and subtractive techniques to construct functional structures on a continuous substrate known as a web, which is continuously transported via multiple rollers.[37] Recent studies have demonstrated the development of integrated R2R processes to produce microstructural devices, flexible electronics, and biomedical components, such as microfluidic devices,[33, 34] solar cells,[35, 36] and integrated immunodetection sensors.[37] Hiltunen et al. demonstrated a R2R thermal imprinting method to fabricate microfluidics for molecular diagnostics that could produce tens of thousands of replicas in an hour,[34] and Liedert et al. reported that the R2R process could fabricate integrated sensors for blood filtration and immunodetection at a speed of 60 devices per hour.[37]

The R2R process of PDMS-based devices has been the focus of extensive research, as PDMS is one of the most popular materials for flexible electronics and microfluidic devices.[39-42] In 2008, Ahn et al. imprinted nanostructures onto a PDMS layer on a PET (polyethylene terephthalate) substrate using a R2R process.[42] Hiltunen et al. developed a R2R fabrication process for PDMS-based microfluidic devices for nucleic acid amplification based on thermal imprinting.[34] Hoang et al. demonstrated room-temperature R2R fabrication of microfluidic devices using specially formulated PDMS.[43] Various manufacturing processes can be integrated into the R2R fabrication of PDMS. For instance, a CO_2 laser engraver was integrated with a R2R setup to pattern a thin PDMS films for a microfluidic artificial lung.[33] Additionally, knife coating of PDMS was utilized in a R2R format for multilayer structures to insulate electronic components during the batch production of large-scale stretchable hybrid devices.[44]

These advancements highlight the potential of R2R process for PDMS-based devices in facilitating the transition from prototypes to commercial products.

In this work, we demonstrate a R2R process for fabricating the self-folding microstructures (**Figure 1**). A PDMS film is stretched and attached to an unstretched PDMS film on a stiff PET carrier layer through the R2R process to produce a self-folding bilayer PDMS film. Patterns are then engraved on the film and released to form 3D microstructures. We demonstrate the fabrication of multiple 3D microstructures, such as hollow spheres or HMCs, finger-like structures, and tubes, with significantly improved throughput compared to our earlier approach based on spin-coating.[10] The HMCs fabricated using the R2R process are successfully validated by demonstrating the successful expansion of mammalian cells.

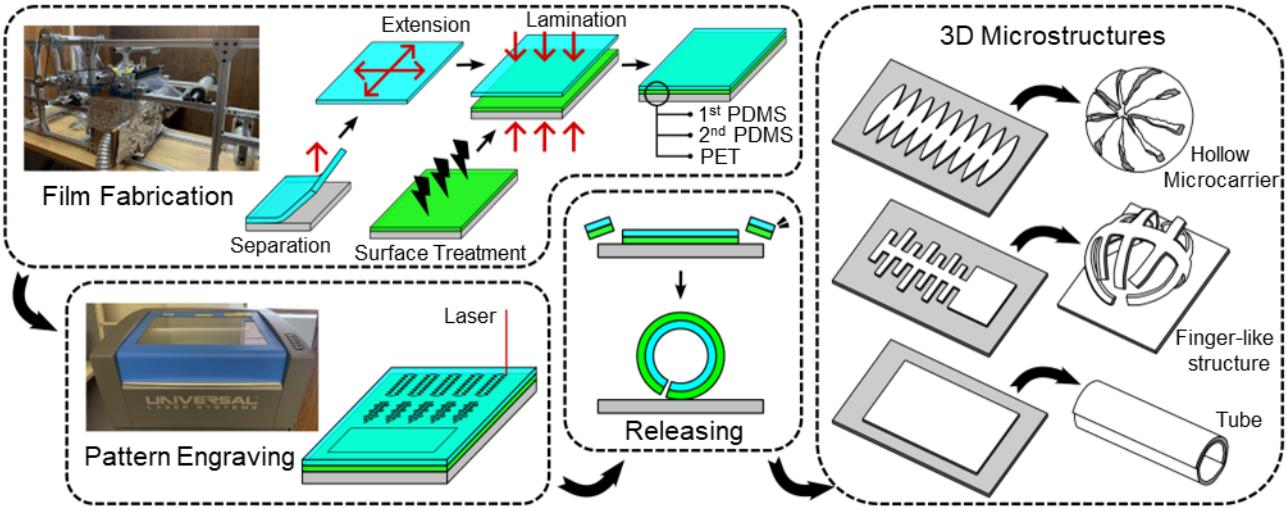

Figure 1. Overview of the R2R manufacturing process. A self-folding bilayer PDMS film was fabricated using the R2R setup and 2D patterns were engraved on the film. The engraved patterns were fully or partially released from the PET carrier to form 3D microstructures.

Materials and Methods

Materials

Pre-cured PDMS films with thicknesses of 20 and 50 μm, which were attached to a 135 μm thick PET carrier layer, were purchased in 24-cm wide, 80-meter rolls (SILPURAN 2030, Wacker Chemie AG, Germany).

Characterization of stretching ratio and ROC

A PDMS film was released from a PET carrier layer and then attached to four PDMS blocks on the isotropic film stretcher (**Figure 2a**). The PDMS blocks were treated with a corona discharger (BD-20AC; 12051A, Electro-Technic Products, USA) before bonding to the PDMS film. The four PDMS blocks were installed on screw-driven guide rails. As the four screws were turned at the same rate, the brackets holding the PDMS blocks were pulled away at the same rate to stretch the film isotopically (**Figure 2b**). Then, another PDMS film on a PET carrier was permanently bonded to the stretched film. After bonding, the combined layer was removed from the stretcher, and thin strips were patterned with a CO_2 laser engraver (VLS2.30, Universal Laser Systems, USA), at the center of the combined layer where the strain was spatially uniform (**Figure 2c**). The engraved patterns were manually released from the PET carrier with tweezers to measure their ROC.

Configuration of R2R setup

As shown in **Figure 3**, on a custom-designed aluminum frame (1515, 80/20, USA), multiple rollers (635132, ServoCity, USA), two motors (1st motor: 638263, ServoCity, USA; 2nd motor: 638162, ServoCity, USA), and two brakes (29LGBE24, Maxcess, USA) were installed along with other electronics. The rotation of the two motors was controlled by a DC motor controller (RoboClaw 2×7A; IMC404, Basicmicro, USA) and rotary encoders (COM-11102 ROHS,

SparkFun, USA). The transmission system of the rollers consisted of aluminum hub gears (615238, ServoCity, USA), sprockets (615126, ServoCity, USA), and chains (615146, ServoCity, USA). The PDMS film was stretched by a deep groove ball bearing (205K-BEARING, VXB, USA) array with rubber wheels (123185, Moxi, USA) on the sides to hold the film edges. The corona dischargers were mounted on a custom bracket moving along a guide rail driven by a linear actuator. The ozone produced during the corona treatment was filtered through a carbon filter (AeroZesh S6 Combo, VIVOSUN, USA).

Fabrication of HMC

The laser engraver was used to engrave the patterns of HMC on the self-folding film. For human embryonic kidney (HEK) 293 cell culture, the engraved film was immersed in a 0.01% poly-L-lysine solution (P4707, Sigma-Aldrich, USA) for one hour and then washed with phosphate-buffered saline (PBS; 10010023, Thermo Fisher Scientific, USA). After surface functionalization, the HMC patterns were manually released with tweezers and sterilized in 70% ethanol.

Expansion of HEK 293 cells

The HEK 293 cells (11625019, Thermo Fisher Scientific, USA) were cultured in tissue culture flasks at 5% CO_2 and 37°C, under humidified conditions. The culture media was Dulbecco's modified eagle medium (DMEM; 12100046, Thermo Fisher Scientific, USA), supplemented with 10% (v/v) fetal bovine serum (FBS; 10437036, Thermo Fisher Scientific, USA), and 1% (v/v) penicillin-streptomycin (P/S; 15140122, Thermo Fisher Scientific, USA).

Cell seeding and culture of HMC

The procedure for cell seeding in HMCs was described in previous work by Ashkan et al.[10] Following the seeding process, the HMCs were placed in a spinner flask (CLS-1430-100, Chemglass, USA) containing 100 mL of culture media and stirred at 25 rpm using a slow-speed stirrer (440811, Cole-Parmer, USA). The spinner flask was aerated with humidified air in the incubator, which was maintained under standard condition (5% CO_2 at 37°C).

Protocol for proliferation assay

The growth of HEK 293 cells in the HMCs was confirmed with two independent methods. In the first method, cell counting kit-8 (CCK-8; CK04, Dojindo, Japan) was utilized following the manufacturer's instructions. The total cell number in the HMCs was recorded on days 2, 3, 4, and 5 of culture. For the second method, cells were harvested at the end of the culture by TrypLE Select (12563029, Thermo Fisher Scientific, USA). Ten HMCs were immersed in 5 mL of TrypLE Select and flushed several times using a serological pipette. The HMCs were incubated overnight at 37°C in the enzyme. Following incubation, the cells were harvested by rinsing the HMCs again with a serological pipette. The HMCs were then examined under a microscope to ensure that no cells remained. The total number of cells in the enzyme was manually counted by using a hemocytometer.

Results and Discussion

Various combinations of the PDMS film thickness and stretching ratios were tested with the isotropic film stretcher, as illustrated in **Figure 2** and detailed in **Table 1**. PDMS strips under the various conditions listed in **Table 1** were shown in **Figure 2d**.

The ROC of the bilayer film was analyzed with Timoshenko's formula:[21, 45-47]

$$\frac{1}{ROC} = \kappa = \frac{6E_a \varepsilon t_a}{E_p t^2}\gamma \qquad (1a)$$

$$\gamma = \frac{(1+\beta)^3}{1+4\alpha\beta+6\alpha\beta^2+4\alpha\beta^3+\alpha^2\beta^4} \qquad (1b)$$

where κ is the bending curvature, ε is the mismatch strain between the active and passive layers, $\alpha = E_a/E_p$ is the ratio of Young's modulus of the active layer E_a and passive layer E_p, $\beta = t_a/t_p$ is the ratio of active layer thickness t_a and passive layer thickness t_p, and t is the total thickness of the bilayer film. For the bilayer PDMS film, where $\alpha = 1$, **Equation 1a** can be simplified to:

$$\frac{1}{ROC} = \kappa = \frac{6\varepsilon t_a}{t^2}(1+\beta)^{-1} \qquad (2)$$

In this work, ε = 6%, 12%, and 16% were tested. The 50 μm PDMS film was used as the active layer to ensure stable and reliable stretching and both of 50 and 20 μm PDMS films were used as the passive layer. As shown in **Figure 2e**, the experimental measurements of the ROC for the PDMS strips under each condition closely matched the results from **Equation 2**. For the same stretching ratio, the strip with a 20 μm passive layer exhibited a smaller ROC compared to the 50 μm passive layer, as the combined bilayer film was thinner. Additionally, the bending curvature, κ, of the PDMS strips showed a positive linear correlation with the stretching ratio (**Figure 2f**). Based on these results, a 50 μm active layer and a 20 μm passive layer with a

stretching ratio around 12% were selected to produce an ROC of around 0.5 mm, matching the radius of the previously developed HMCs.[10]

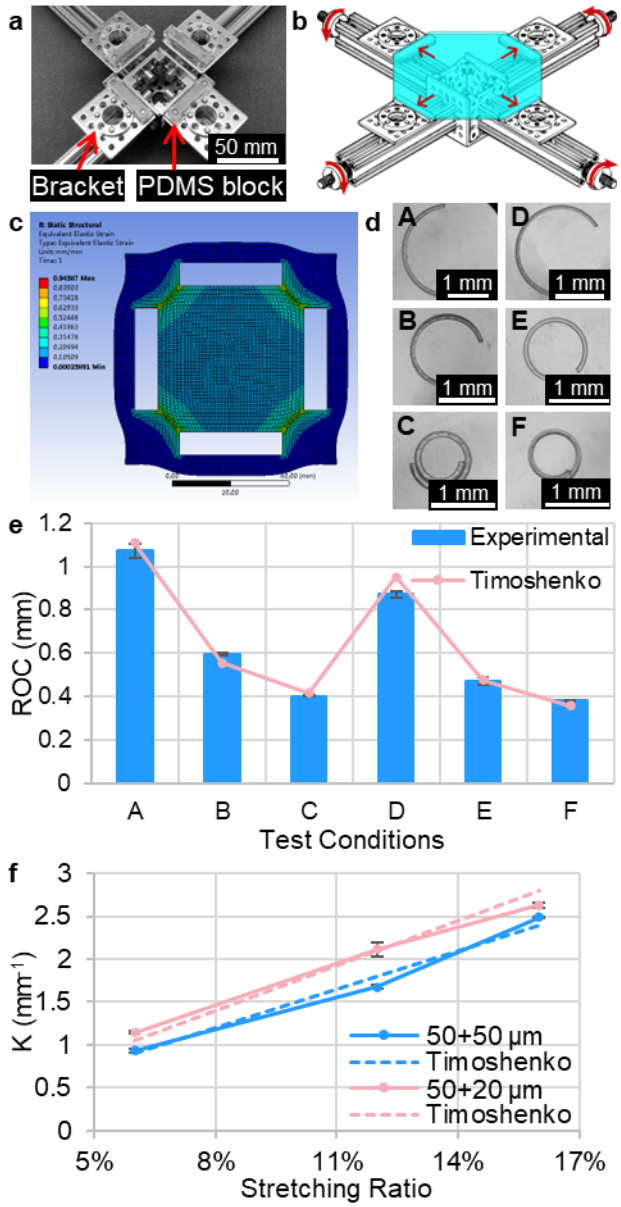

Figure 2. Characterization of ROC. a) Photograph and b) operational of the isotropic film stretcher. c) Finite element analysis shows a uniform strain in the center of the stretched PDMS film. d) Photographs of the released PDMS strips. Measured e) ROC and f) bending curvature (solid line) of released PDMS strips showing good agreement with Timoshenko's formula (dotted line).

Strips	A	B	C	D	E	F
Stretch (%)	6%	12%	16%	6%	12%	16%
Active layer thickness (µm)	50	50	50	50	50	50
Passive layer thickness (µm)	50	50	50	20	20	20
ROC (mm)	1.07± 0.031	0.60± 0.007	0.40± 0.002	0.87± 0.016	0.47± 0.019	0.38± 0.004

Table 1. ROC of released PDMS strips under each condition.

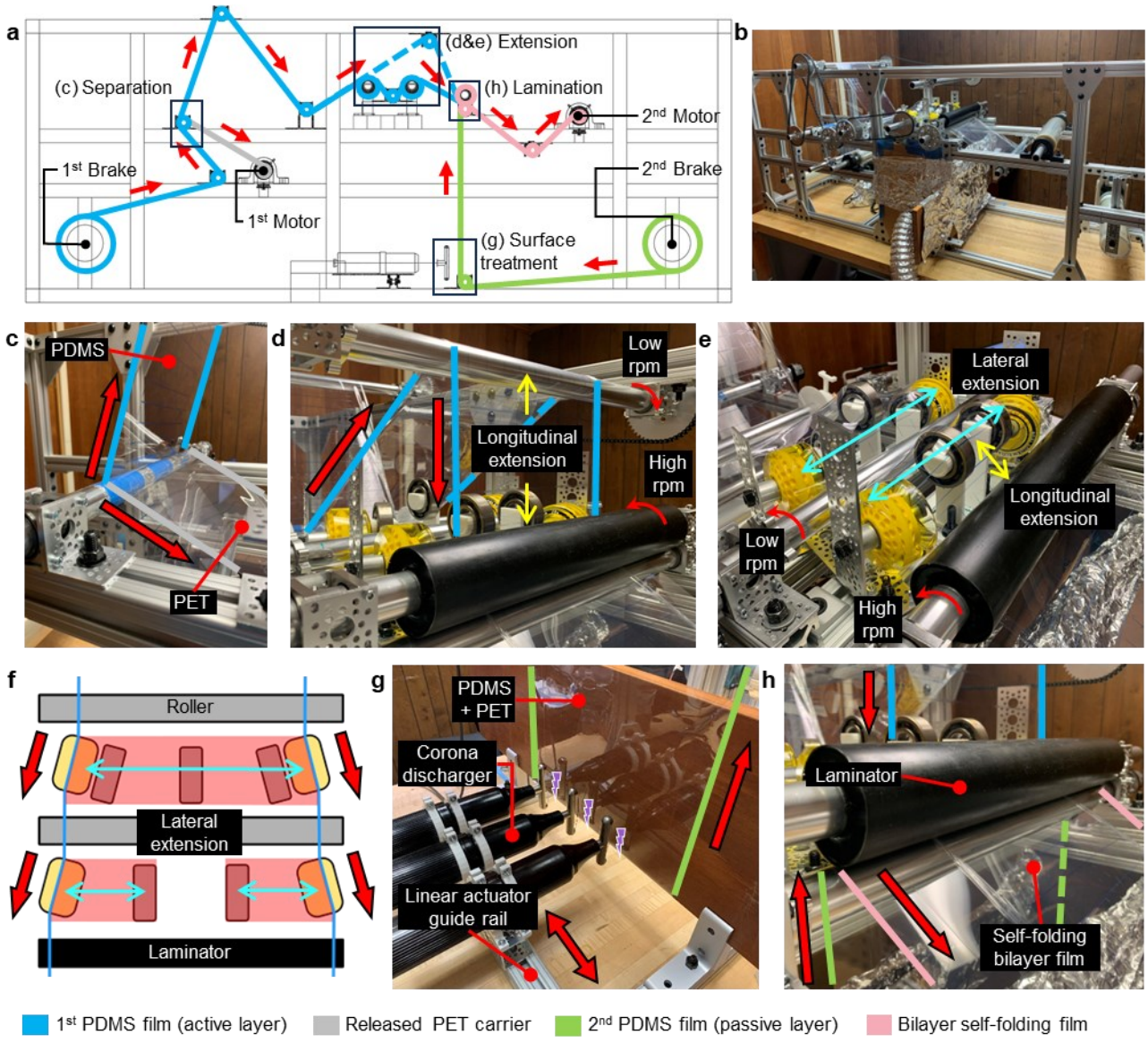

Figure 3. R2R fabrication setup of self-folding film. a) Schematic diagram and b) photograph of the R2R setup. c) 1st PDMS film was released from PET carrier in the separation section. d) 1st PDMS film was stretched longitudinally by higher web speed in the extension section in uniaxial stretching mode. e) 1st PDMS film is stretched laterally using the f) bearing array and longitudinally by a higher web speed in the extension section in biaxial stretching mode. g) 2nd PDMS film was treated by the corona dischargers in the surface treatment section. h) 1st and 2nd PDMS films were bonded together in the lamination section to form the self-folding film.

The R2R fabrication setup for self-folding film had four primary modules: separation, extension, surface treatment, and lamination, as shown in **Figure 3a**. The roll of the 1st PDMS film or the active layer was held at the 1st brake and that of the 2nd PDMS film or the passive layer was held at the 2nd brake. Together with the 1st brake, the 1st motor, rotating at 1 rpm,

produced tension on the film before separation. The 2nd motor ran 1–5% faster than the 1st motor, to create a speed difference for longitudinal film extension, as well as the tension required for lateral extension on the bearing array (**Figure 3e & 3f**) and the lamination.

In the separation section (**Figure 3c)**, the 1st PDMS film was released and then transferred to the extension section, while the PET carrier was collected by the roller attached to the 1st motor. The two rollers after the separation point were chained to the 1st motor and rotated at the same rpm, so that the separated PDMS film could be transported to the extension section without increased tension.

After separation, the 1st PDMS film was then stretched in the extension section. Our setup allows for both uniaxial stretching (**Figure 3d**) and biaxial stretching (**Figure 3e**). In the uniaxial stretching mode, the 1st PDMS film was fed to the roller at the top of the extension section and stretched by the difference in speed between the two motors. The speed differences of 1% and 5% would stretch the film longitudinally by 13% and 17%, respectively. In the biaxial stretching mode, the film was stretched laterally by the bearing array illustrated in **Figure 3f** and stretched longitudinally by the speed difference between the two motors. The bearing array consisted of two sets of bearings: the first set of bearings was used to pre-stretch the middle area of the PDMS film, while the second set of bearings was used to stretch the sides of the film. The lateral extension ratio was controlled by the location and angle of the side bearings. With the side bearing angle of 20° and the 5% speed difference of the two motors, the 1st PDMS film was stretched by 15% in the lateral direction and 14% in the longitudinal direction, respectively.

In the surface treatment section, the 2nd PDMS film on PET carrier was unrolled by the 2nd motor and then treated by three corona dischargers to enhance bonding strength,[48-51] as shown in **Figure 3g**. In order to activate the entire width of the 2nd PDMS film, the corona dischargers moved back and forth along a guide rail driven by a linear actuator.

In the lamination step, the stretched 1st PDMS film was bonded to the 2nd PDMS film, as shown in **Figure 3h**, and the bonded bilayer PDMS film on the PET carrier was collected by the roller attached to the 2nd motor. To minimize air trapping between the two films, the angle between the 2nd PDMS film and the produced self-folding film was adjusted so that the combined film wrapped more angle around the bottom lamination roller.

The R2R fabrication process significantly improved the throughput of the self-folding film compared to conventional spin-coating methods. The width of the isotropic stretching area was 11.5 cm in the middle of the 1st PDMS film, which was approximately 50% of the original width of the film. At 5% speed difference between the two motors, the web speed of the R2R setup was 8.38 cm/min, leading to a production speed of 96.35 cm^2/min for the self-folding film. In comparison, considering equipment usage, logistics, and our earlier experiences, an operator could produce up to eight 4-inch wafers in two days using the spin-coating process, fabricating the self-folding film with a total area of 648 cm^2.

Various 3D structures could be made from the R2R fabricated self-folding film, as shown in **Figure 4**. To engrave the 2D patterns, a CO_2 laser engraver was used after the R2R process. The output power of the engraver was carefully optimized to minimize the kerf and to only cut through the bilayer PDMS film without damaging the PET carrier (Supplementary Figure S1).

The kerf of the laser engraver was about 100 μm. The PDMS film around the patterns was then removed, leaving only the patterns on the PET carrier. At this stage, the top surface of the 2D patterns could be selectively functionalized or modified, as it would become the inner surface of the folded 3D structures after releasing from the PET carrier. This allowed users to easily access the inner surface during the fabrication process, making it more convenient for users to fabricate 3D structures for specific applications. Moreover, the outer surface of the film could be further modified, as it would be exposed after the releasing process. **Figure 4a** showed the HMC patterns engraved on the self-folding film fabricated by the R2R setup with biaxial stretching mode. After being released from the PET carrier, these patterns folded into hollow microspheres (**Figure 4b**). To demonstrate the uniformity of the self-folding film, the diameter of 96 HMCs were measured, as shown in **Figure 4c**. These HMCs were engraved on a 121 cm^2 self-folding film and the engraving positions were randomly selected. The average diameter was 1.05 ± 0.024 mm. **Figure 4d** showed the pattern engraved on the self-folding film to form finger-like structures (**Figure 4e**). The bottom of the pattern was still connected to the film, allowing the structure to grab and hold a small spherical target near the substrate. With the self-folding film fabricated by the R2R setup with uniaxial stretching mode, the rectangular patterns were used to create tubular structures (**Figure 4f & 4g)**. We characterized the diameter of the tubes with rectangular patterns of different sizes and stretching ratios. As shown in **Table 2**, the ROC of the tube increased from 0.74 to 0.99 mm if the pattern width increased from 6 to 10 mm at 13% stretching ratio, whereas the ROC of the tube remained approximately 0.6 mm if the stretching ratio was 17%.

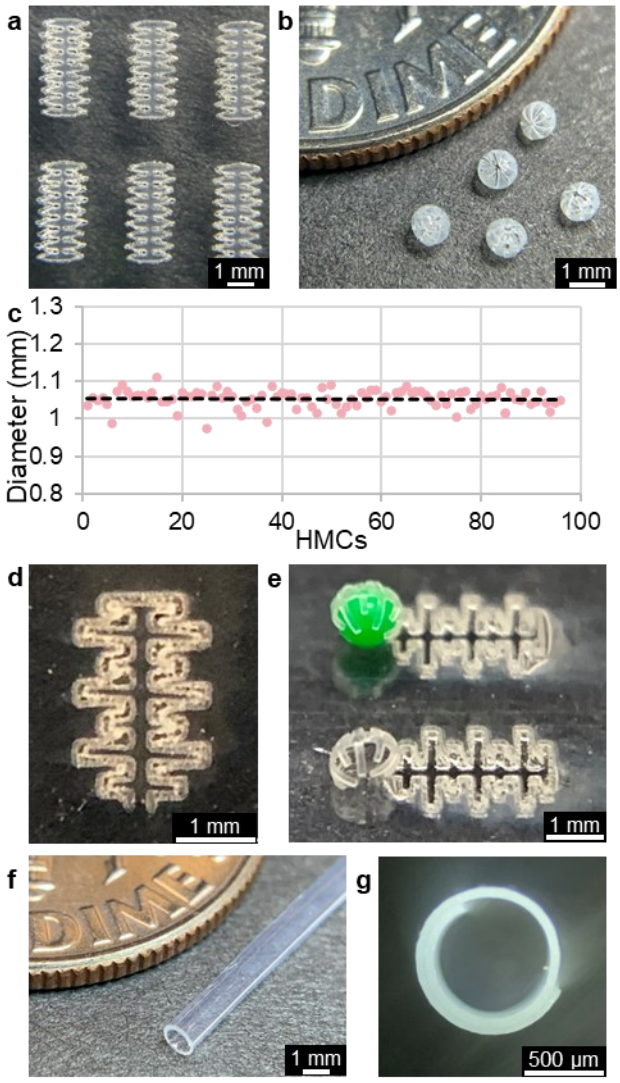

Figure 4. Self-folding 3D microstructures. a) HMC patterns (biaxially stretched) on the PET carrier prior to release. b) Released HMCs. c) The diameter of 96 HMCs measured was 1.05 ± 0.024 mm. d) Pattern for finger-like structure (biaxially stretched) on the PET carrier prior to release. e) Finger-like structure clutching a 1-mm diameter microsphere (top) and an empty finger-like structure (bottom). f) Released tube. g) Cross-sectional view of the tube self-folded from a rectangular pattern (uniaxially stretched).

Tubes	G	H	I	J	K
Stretch (%)	13%	13%	13%	13%	13%
Length (mm)	30	30	30	60	120
Width (mm)	6	8	10	10	10
ROC (mm)	0.74± 0.020	0.94± 0.008	0.98± 0.061	0.89± 0.024	0.99± 0.070
Tubes	**L**	**M**	**N**	**O**	**P**
Stretch (%)	17%	17%	17%	17%	17%
Length (mm)	30	30	30	60	120
Width (mm)	4	5	6	6	6
ROC (mm)	0.60± 0.012	0.59± 0.008	0.59± 0.008	0.59± 0.011	0.60± 0.004

Table 2. ROC of released tubes under each condition.

To validate the functionality of the self-folding HMCs, we demonstrated the expansion of HEK 293 cells in the HMCs for five days. A self-folding film with an area of 35 cm^2 was used to fabricate 300 HMCs. The HMC patterns attached to the PET carrier were treated with a 0.01%

poly-L-lysine solution to enhance cell attachment, resulting in a treated inner surface and an unmodified outer surface of the HMCs upon release. As only the inside of the HMCs was treated, HEK 293 cells were only attached to and cultured on the inner surface of the HMC (**Figure 5a**), where the cells could be shielded from the shear stress of the spinner flask.[10] The phase contrast images of HEK 293 cells inside the HMCs are displayed in **Figure 5b**. Active proliferation was observed for five days, and the cells exhibited exponential growth throughout the culture period (**Figure 5d)**. At the end of the culture, the number of HEK 293 cells within the HMCs was quantified, as shown in **Figure 5e**. For measurement by CCK-8, 5.99×10^3 cells were counted per HMC, leading to a cell doubling time of 26.51 hours. For cells dissociated with TrypLE Select and manually counted using a hemocytometer, 5.38×10^3 cells were counted per HMC, resulting in a cell doubling time of 27.46 hours.

While the proposed R2R setup exhibited sufficient throughput for proof-of-concept studies, there is a potential to substantially enhance its yield, possibly on an industrial scale. Firstly, the web speed can be further increased to boost output. In this work, the web speed was set to the minimum and the R2R setup operated in a quasi-static condition to facilitate development and optimization. Although this had not been attempted earlier, we believe that the web speed can be increased several times without major issues. Secondly, the stretching module can be optimized to expand the usable area of the combined PDMS film. In this study, about 4 cm of the web width on each side was used to hold and laterally stretch the 50 μm PDMS film in the extension section, and about 3 cm of the web on each side was not usable due to non-uniform stretching. Using wider PDMS rolls or improving how the bearing array holds the film edge can enhance the usage of raw materials and overall productivity. Finally, integrating a galvo-

type laser engraver, as demonstrated in an earlier study,[33] would increase overall throughput, as the engraving speed of a galvo-type laser engraver is several times higher than that of the gentry-type laser engraver used in this study.

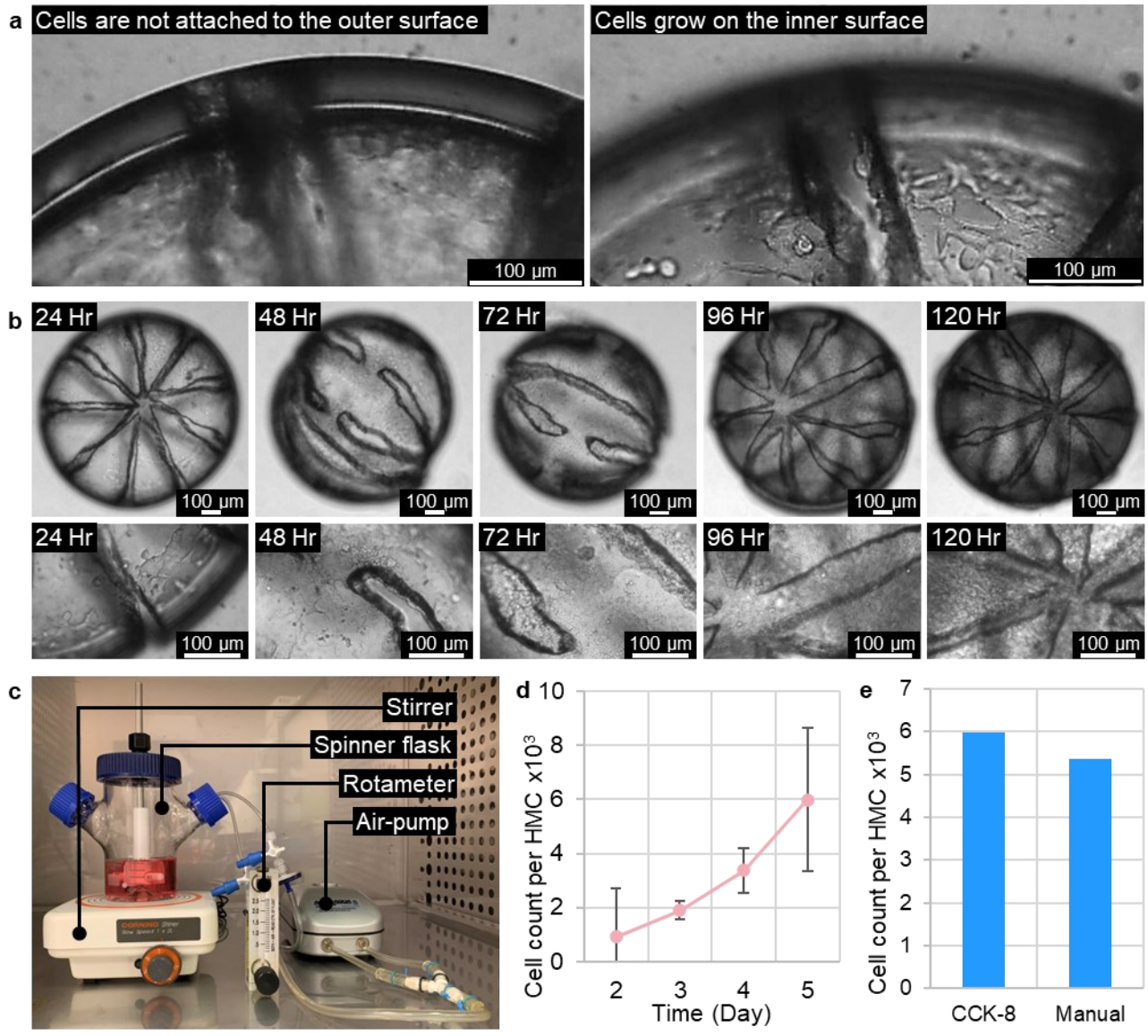

Figure 5. Culture of HEK 293 cells in HMCs. a) Phase-contrast images focused on the unmodified outer surface (left) and poly-L-lysine treated inner surface (right) of a HMC, 24 hours after cell seeding. b) HEK 293 cells showed active growth in HMCs over 5 days. c) Cell culture setup in a CO_2 incubator. d) Cell count in HMCs recorded at 48, 72, 96, and 120 hours. e) The number of cells in HMCs was measured on day-5 using colorimetric assays with CCK-8, and manual counting after cell harvest.

Utilizing gravure or blade coating to produce PDMS films in the R2R setup, as demonstrated in earlier literature,[34, 43, 44] would broaden material options and enable control of film thickness. Moreover, these coating techniques can be used to add a sacrificial layer between the PDMS layer and the PET carrier for self-releasing. For instance, Kawakami et al. showed that a gravure coater and a heater could fabricate a sacrificial layer on the PET carrier in the R2R process for releasing large-scale stretchable hybrid devices.[44] In our previous study, Ashkan et al. used photoresist as the sacrificial layer to release HMCs, where the photoresist was easily soluble in ethanol.[10] We believe that the use of a sacrificial layer would allow the use of the releasing technique from our earlier study and significantly streamline the fabrication process of HMCs or similar microstructures.

The size of the microstructures depends on the ROC of the self-folding film, which in turn is determined by various factors, including thickness and stretching ratio of films. In this study, pre-cured PDMS films were available in thicknesses from 20 μm to 400 μm, and stretching ratios were varied between 6% and 16%. Applying these parameters to Equation 2, the minimum achievable ROC would be 0.16 mm, obtained with 20 μm thick films and a 16% stretch. Conversely, the maximum ROC would be 8.8 mm with 400 μm films and a 6% stretch. To achieve smaller ROC, either the stretching ratio must be increased, potentially by enhancing the extension module shown in Figure 3e, or thinner films below 20 μm must be used.

The released microstructures were very stable and showed no signs of mechanical degradation for over several months (Supplementary Figure S2). However, microstructures fabricated with a self-folding film aged for several months exhibited significantly larger ROC compared to

those made with a freshly produced film (Supplementary Figure S2). This phenomenon can be attributed to stress relaxation, a process in which viscoelastic materials, especially polymers, relieve stress when subjected to constant strain.[52] The PDMS bilayer is kept flat before being released from the rigid PET carrier, leading to a gradual loss of tensile stress over time. Fortunately, stress relaxation in PDMS occurs very slowly at room temperature;[53] thus, changes in the ROC are not observable within a couple of weeks.

Due to the spatially uniform tensile stress within the self-folding film, the resulting microstructures are exclusively spherical or tubular in shape. By selectively engraving the active layer of the self-folding film, the intensity and direction of the tensile stress can be precisely modulated, enabling the fabrication of microstructures with diverse shapes beyond tubes and spheres.

Conclusion

In this study, we presented a R2R process for fabricating self-folding 3D microstructures. A R2R setup was developed to produce self-folding films that could fold biaxially or uniaxially. The R2R process significantly increased throughput compared to the previous fabrication process based on spin-coating and baking, reducing the fabrication time for self-folding films from two days to just minutes. We demonstrated three 3D microstructures folded by the self-folding films: hollow microspheres (HMCs), finger-like structures, and tubular structures. HEK 293 cells were successfully cultured in the HMCs in the spinner flask and efficiently harvested. The R2R-fabricated self-folding film allowed easy and selective modification of the inner

surface of the HMCs to enhance cell attachment. Self-folding technology offers significant promise for creating innovative microstructures with applications in advanced bioreactors, tissue engineering, drug delivery, and cellular research. The demonstrated R2R fabrication setup would facilitate the successful commercialization of self-folding microstructures.

Author Contributions

T.W. and A.M developed the R2R setup. T.W. collected experimental data. K.P. proposed the project and provided guidance for the experiments. The manuscript was written by T.W. and K.P.

Conflict of Interest

Louisiana State University owns patents on hollow microcarrier technology.

Data availability

Data for this article, including an ANSYS project file for finite element analysis, are available at Open Science Framework at https://doi.org/10.17605/OSF.IO/ZBH72.

Acknowledgements

This material is based upon work supported by the National Science Foundation under Grant No. 1848251 and the Louisiana Board of Regents under Grant No. LEQSF(2023-24)-RD-D-02.

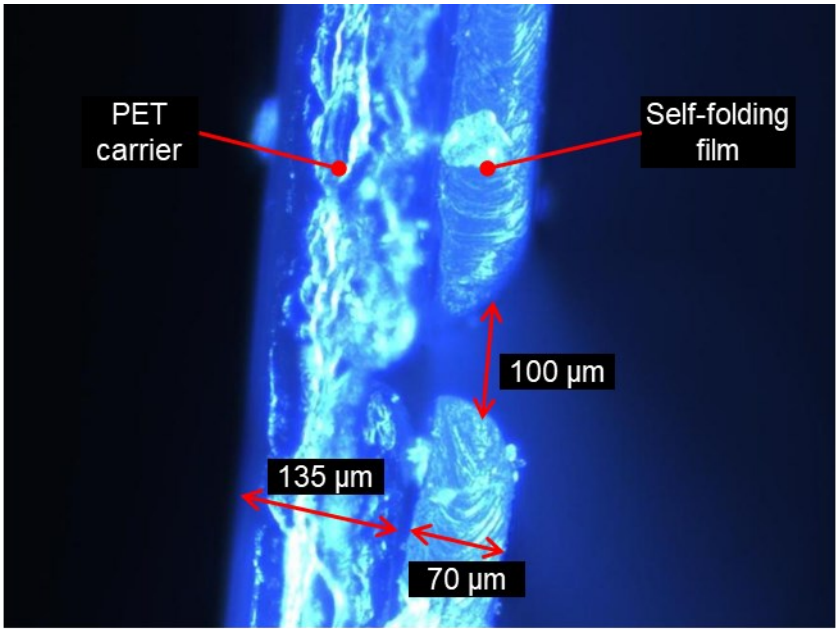

Supplementary Figure S1. Cross-sectional view of laser engraver cutting profile. The cut-width (kerf) is about 100 µm. The cut-depth is about 70 µm.

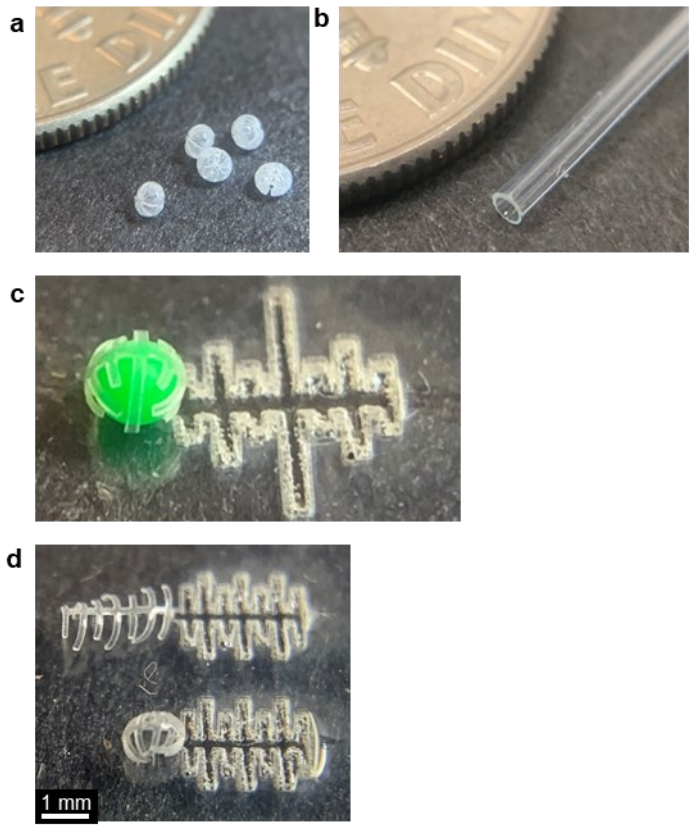

Supplementary Figure S2. a), b), c) Self-folding 3D microstructures after being stored in air for 11 months. No sign of deformation can be observed. d) The self-folding film was produced 12 months ago. The bottom pattern was engraved and released about 11 months ago, retaining its original shape. The top pattern was engraved about 11 months ago and released a week ago, demonstrating a loss of self-folding behavior due to stress relaxation.

References

1. T. G. Leong, A. M. Zarafshar and D. H. Gracias, *small*, 2010, **6**, 792-806.
2. C. L. Randall, E. Gultepe and D. H. Gracias, *Trends in biotechnology*, 2012, **30**, 138-146.
3. L. Ionov, *Soft Matter*, 2011, **7**, 6786-6791.
4. R. Fernandes and D. H. Gracias, *Advanced drug delivery reviews*, 2012, **64**, 1579-1589.
5. J. Voldman, M. L. Gray and M. A. Schmidt, *Annual review of biomedical engineering*, 1999, **1**, 401-425.
6. D. H. Gracias, V. Kavthekar, J. C. Love, K. E. Paul and G. M. Whitesides, *Advanced Materials*, 2002, **14**, 235-238.
7. T. G. Leong, B. R. Benson, E. K. Call and D. H. Gracias, *Small*, 2008, **4**, 1605-1609.
8. K. Suzuki, H. Yamada, H. Miura and H. Takanobu, *Microsystem Technologies*, 2007, **13**, 1047-1053.
9. A. Azam, K. E. Laflin, M. Jamal, R. Fernandes and D. H. Gracias, *Biomedical microdevices*, 2011, **13**, 51-58.
10. A. YekrangSafakar, A. Acun, J. W. Choi, E. Song, P. Zorlutuna and K. Park, *Biotechnology and bioengineering*, 2018, **115**, 1717-1728.
11. G. Stoychev, N. Puretskiy and L. Ionov, *Soft Matter*, 2011, **7**, 3277-3279.
12. J. Kim, C. Kim, Y. Song, S.-G. Jeong, T.-S. Kim and C.-S. Lee, *Chemical Engineering Journal*, 2017, **321**, 384-393.
13. S. Zakharchenko, N. Puretskiy, G. Stoychev, M. Stamm and L. Ionov, *Soft Matter*, 2010, **6**, 2633-2636.
14. S. Zakharchenko, E. Sperling and L. Ionov, *Biomacromolecules*, 2011, **12**, 2211-2215.
15. G. Huang, Y. Mei, D. J. Thurmer, E. Coric and O. G. Schmidt, *Lab on a Chip*, 2009, **9**, 263-268.
16. V. Luchnikov, O. Sydorenko and M. Stamm, *Advanced Materials*, 2005, **17**, 1177-1182.
17. L. Ionov, *Macromolecular chemistry and physics*, 2013, **214**, 1178-1183.
18. G. Stoychev, S. Turcaud, J. W. Dunlop and L. Ionov, *Advanced Functional Materials*, 2013, **23**, 2295-2300.
19. A. Khandelwal, Z. Ren, S. Namiki, Z. Yang, N. Choudhary, C. Li, P. Wang, Z. Mi and X. Li, *ACS Applied Materials & Interfaces*, 2022, **14**, 29014-29024.
20. A. de Leon, A. C. Barnes, P. Thomas, J. O'Donnell, C. A. Zorman and R. C. Advincula, *ACS Applied Materials & Interfaces*, 2014, **6**, 22695-22700.
21. J. Cui, J. G. Adams and Y. Zhu, *Smart Materials and Structures*, 2018, **27**, 055009.
22. T. S. Kelby, M. Wang and W. T. Huck, *Advanced Functional Materials*, 2011, **21**, 652-657.
23. Y. Liu, J. K. Boyles, J. Genzer and M. D. Dickey, *Soft matter*, 2012, **8**, 1764-1769.
24. E. Smela, O. Inganäs and I. Lundström, *Science*, 1995, **268**, 1735-1738.
25. C. Py, P. Reverdy, L. Doppler, J. Bico, B. Roman and C. N. Baroud, *Physical review letters*, 2007, **98**, 156103.
26. J. Li, J. Zhang, W. Gao, G. Huang, Z. Di, R. Liu, J. Wang and Y. Mei, *Advanced Materials*, 2013, **25**, 3715-3721.
27. E. W. Jager, O. Inganas and I. Lundstrom, *Science*, 2000, **288**, 2335-2338.
28. M. Smolka, S. Ruttloff, D. Nees, C. Prietl, V. Satzinger, B. Lamprecht, P. Hütter, J. Hesse, G. Kokkinis and G. Kriechhammer, 2018.
29. H. He, J. Guan and J. L. Lee, *Journal of Controlled Release*, 2006, **110**, 339-346.
30. C. L. Randall, Y. V. Kalinin, M. Jamal, T. Manohar and D. H. Gracias, *Lab on a Chip*, 2011, **11**, 127-131.
31. D. H. Gracias, J. Tien, T. L. Breen, C. Hsu and G. M. Whitesides, *science*, 2000, **289**, 1170-1172.

32. M. Jamal, N. Bassik, J.-H. Cho, C. L. Randall and D. H. Gracias, *Biomaterials*, 2010, **31**, 1683-1690.
33. A. Zhang, K. Tharwani, J. Wang, G. K. Seilo, M. Atie and J. A. Potkay, *Lab on a Chip*, 2024.
34. J. Hiltunen, C. Liedert, M. Hiltunen, O.-H. Huttunen, J. Hiitola-Keinänen, S. Aikio, M. Harjanne, M. Kurkinen, L. Hakalahti and L. P. Lee, *Lab on a Chip*, 2018, **18**, 1552-1559.
35. J. E. Kim, S. S. Kim, C. Zuo, M. Gao, D. Vak and D. Y. Kim, *Advanced Functional Materials*, 2019, **29**, 1809194.
36. D. Angmo, G. DeLuca, A. D. Scully, A. S. Chesman, A. Seeber, C. Zuo, D. Vak, U. Bach and M. Gao, *Cell Reports Physical Science*, 2021, **2**.
37. C. Liedert, L. Rannaste, A. Kokkonen, O.-H. Huttunen, R. Liedert, J. Hiltunen and L. Hakalahti, *ACS sensors*, 2020, **5**, 2010-2017.
38. T.-Y. Yang, Y. Y. Kim and J. Seo, *APL Materials*, 2021, **9**.
39. G. M. Whitesides, *nature*, 2006, **442**, 368-373.
40. L. Gervais, N. De Rooij and E. Delamarche, *Advanced materials*, 2011, **23**, H151-H176.
41. C. D. Chin, V. Linder and S. K. Sia, *Lab on a Chip*, 2012, **12**, 2118-2134.
42. S. H. Ahn and L. J. Guo, *Advanced materials*, 2008, **20**, 2044-2049.
43. T. Hoang, H. Truong, J. Han, S. Lee, J. Lee, S. Parajuli, J. Lee and G. Cho, *Materials Today Bio*, 2023, **23**, 100838.
44. H. Kawakami, K. Nagatake, S. Ni, F. Nakamura, T. Takano, K. Murakami, I. Ohara, Y. Isano, R. Matsuda and H. Suwa, *Advanced Materials Technologies*, 2024, 2400487.
45. S. Timoshenko, *Josa*, 1925, **11**, 233-255.
46. M. Huang, P. Rugheimer, M. Lagally and F. Liu, *Physical Review B—Condensed Matter and Materials Physics*, 2005, **72**, 085450.
47. J. Zang and F. Liu, *Applied Physics Letters*, 2008, **92**.
48. M. Goldman, A. Goldman and R. Sigmond, *Pure and Applied Chemistry*, 1985, **57**, 1353-1362.
49. D. C. Duffy, J. C. McDonald, O. J. Schueller and G. M. Whitesides, *Analytical chemistry*, 1998, **70**, 4974-4984.
50. K. Haubert, T. Drier and D. Beebe, *Lab on a Chip*, 2006, **6**, 1548-1549.
51. A. Borók, K. Laboda and A. Bonyár, *Biosensors*, 2021, **11**, 292.
52. M. Wang and C. Wang, *Reference Module in Biomedical Sciences: Encyclopedia of Biomedical Engineering*, 2019.
53. H. Zhang, C. Cai, W. Liu, D. Li, J. Zhang, N. Zhao and J. Xu, *Scientific reports*, 2017, **7**, 11833.